Role of Guest Molecules on the Hydrate Growth at Vapor-Liquid Interfaces

Dongsheng Bai

State Key Laboratory of Heavy Oil Processing, School of Chemical Engineering, China University of Petroleum, Beijing 102249, China

Division of Molecular and Materials Simulation, State Key Laboratory of Organic-Inorganic Composites, Beijing University of Chemical Technology, Beijing 100029, China

Bei Liu and Guangjin Chen

State Key Laboratory of Heavy Oil Processing, School of Chemical Engineering, China University of Petroleum, Beijing 102249, China

Xianren Zhang and Wenchuan Wang

Division of Molecular and Materials Simulation, State Key Laboratory of Organic-Inorganic Composites, Beijing University of Chemical Technology, Beijing 100029, China

Systematic molecular dynamics simulations have been performed to illustrate the roles of guest molecules played in the process of hydrate growth at vapor-liquid interfaces. In our simulations, guest molecules are represented by a commonly used single-site Lennard–Jones model, and the roles of guest molecules on hydrate growth have been investigated separately from the effect of water–guest molecule attractive interaction ε and that of molecular size σ, respectively. Our simulation results demonstrate that the water-guest molecule attraction regulates the pathway and rate of nucleus growth, whereas the size of guest molecules determines the dynamically preferable structure. © 2013 American Institute of Chemical Engineers AIChE J, 59: 2621–2629, 2013
Keywords: molecular dynamics simulation, gas hydrate, guest molecule, growth, attraction interaction

Introduction

Gas hydrates are a special class of nonstoichiometric clathrate compounds in which water molecules form cage-like cavities to encapsulate gas molecules.[1] Several types of hydrate lattice structures have been found in nature, including well-known sI (cubic), sII (cubic), sH (hexagonal) structure,[2] and a newly found type of hydrate structure called HS-1(hexagonal) structure.[3,4] Due to their geological importance and potential industrial applications, gas hydrates have been extensively studied in recent years.[5–11]

It is well-known that many small inorganic or organic guest molecules can form gas hydrates, and those simple molecules span a large range of molecular size and solubility in water. For example, hydrates could be used potentially for hydrogen storage,[12–14] just like other energy materials in the form of hydrate (e.g., methane, ethane, and other small hydrocarbon molecules). In addition, hydrogen sulphide (H_2S) hydrates can be used to adjust the formation and decomposition of methane hydrates because of their high nucleation rate.[15,16] Tetrahydrofuran molecules can occupy the large cages in sII hydrates and hence can stabilize gas

hydrates by forming binary hydrates with other gas component.[7] Xe hydrate could be applied potentially for the long-term storage of proteins or other biologically active materials.[17]

A fundamental question in the gas hydrate then arises: what is the role of guest molecules affecting the structure, nucleation, and growth of gas hydrate? To deal with this question, molecular simulation technique has become a powerful tool to provide molecular details of hydrate nucleation and growth process. Molecular simulation has been applied to investigate the effects of guest molecules on the properties of gas hydrate. In recent studies, Jiang and Jordan[18] compared the properties of Xe, CH_4, and CO_2 hydrates by molecular dynamics (MD) simulations. They pointed out that the host-guest coupling is most important for CO_2 hydrate, CO_2, and Xe hydrates that have lower speed of sound and lower thermal conductivities than CH_4 hydrate or the empty lattice. As to the effects of guest molecules on the nucleation of hydrates, it is noticed that most simulation studies are based on CH_4 hydrates,[19–23] and several studies are based on some other gas molecules. By using a coarse-grained model, Jacobson et al.[24] performed a series of MD simulations to elucidate the mechanisms of the nucleation of hydrates. The model guest molecules they used can span a large range of solubility in water and encompass sizes which can stabilize each type of hydrate structure.

Correspondence concerning this article should be addressed to G. Chen at jchen@cup.edu.cn.

As to the role of guest molecules on hydrate growth, however, no systematical research has been done. This is partly ascribed to the difference of experimental conditions or molecular models used in different studies. As a result, although the investigations provide important insights, the detailed role of guest molecules on the growth of gas hydrate is not well-understood. In this work, extensive MD simulations were performed to explore systematically how the properties of guest molecules affect the mechanisms of hydrate growth at the vapor-liquid interface.

Model and Simulation Method

In this work, MD simulations were performed by using LAMMPS,[25] an open source program for massively parallel simulations. In our simulations, the extensively studied TIP4P water model[26] was used, and the rigidity of molecules was constrained by SHAKE algorithm.[27] Guest molecules were represented by a commonly used single-site Lennard–Jones (LJ) model $U_{LJ}(r) = 4\varepsilon\left[\left(\frac{\sigma}{r}\right)^{12} - \left(\frac{\sigma}{r}\right)^{6}\right]$, where ε is the depth of potential well, σ is the collision diameter, and r is the distance between particles. The depth of the potential well ε can be related to the solubility of the guest molecules in water, and the characteristic size σ can represents the size of the guest molecules. By changing the parameters of LJ model, that is (ε, σ), we investigated how the water–guest molecule interaction and the size of the guest molecules affect the hydrate growth, both simultaneously and separately. The LJ parameters of the guest molecules we studied in this work are listed in Figure 1. In general, the chosen LJ parameters of guest molecules (ε, σ) span a wide range, covering almost all the guest molecules that can form hydrates. Several representative sample points labeled by (ε_i, σ_j) with $i, j = 1, 2, 3$ are particularly discussed in the text for clarity (see Figure 1). Note that, in this work, we set $\varepsilon_1 = 0.65$ kJ/mol, $\varepsilon_2 = 1.45$ kJ/mol, $\varepsilon_3 = 2.25$ kJ/mol, $\sigma_1 = 2.8$ Å, $\sigma_2 = 4.2$ Å, and $\sigma_3 = 5.6$ Å, respectively. The unlike parameters of LJ were obtained by the Lorentz–Berthelot mixing rule. A cutoff radius of 12.0 Å was used for the short-ranged interactions, whereas the long-ranged interactions were calculated by the pppm algorithm.[28]

The initial configuration contained a vapor-liquid interface within a simulation box of $7.47 \times 7.47 \times 6.22$ nm^3 (equals to $6 \times 6 \times 5$ unit cells of perfect sI hydrate), as shown in Figure 2. Periodic boundary conditions were imposed in all the three Cartesian directions. To prepare the initial configurations, 4000 H$_2$O molecules were first placed randomly on the lower half of the simulation box and 700 guest molecules were set on the upper half.

As the first step, we need to generate initial hydrate nuclei for different guest molecules before studying hydrate growth. Although the question of where hydrate growth takes place has not been fully resolved, both experimental[29–31] and molecular simulation studies[32,33] show that hydrate nucleation usually occurs at gas-water interface. An "interface hypothesis" has been proposed by Rodger[34] and Kvamme,[35] and they suggested that hydrate nucleation occurs at interfaces by forming hydrate cages. The hypothesis is supported by recent molecular simulation results[32] that the lifetime of hydrate cages increases significantly for those at the interface on the water side. Nucleation at the interface can be ascribed to the lower free energy for hydrate formation and the availability of guest molecules at the interface.
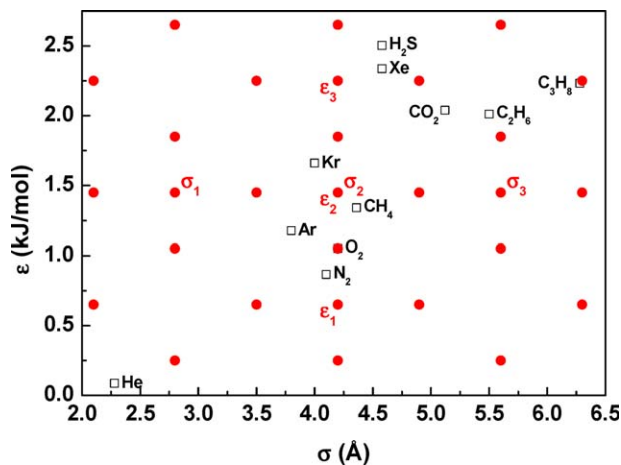

Figure 1. Lennard–Jones parameters of guest molecules investigated in this work.

Red solid dots represent the guest molecules we studied. The range of the LJ parameters can cover almost all the guest molecules that can form hydrates. To compare with experimental results, the LJ parameters of some commonly used guest molecules are also shown in the figure (black hollow squares). Several representative sample points denoted by (ε_i, σ_j) with $\varepsilon_1 = 0.65$ kJ/mol, $\varepsilon_2 = 1.45$ kJ/mol, $\varepsilon_3 = 2.25$ kJ/mol, $\sigma_1 = 2.8$ Å, $\sigma_2 = 4.2$ Å, and $\sigma_3 = 5.6$ Å, are also given in the figure. [Color figure can be viewed in the online issue, which is available at wileyonlinelibrary.com]

In our study, typical initial configurations with a small seed of the gas hydrate embedded in the interface layer were nucleated using the following procedure. To save the computational resource, we performed constrained NVT simulation runs from the initial two-phase system with a constraint that ignores the effect of environmental fluctuation. Different from the normal (unconstraint) MD simulation, the constrained MD forces all the molecules, except for those in a cubic region of $2.5 \times 2.5 \times 2.5$ nm^3 (from 3.75 to 6.25 nm in x axis, from 2.50 to 5.00 nm in y axis, and from 1.25 to 3.75 nm in z axis), to be frozen. The location and size of the cubic region are illuminated in Figure 2. In practice, for a specific type of guest molecules, a series of NVT simulation runs at 255 K, in which a constrained MD run in 2 ns was followed by a 500 ps normal (unconstrained) MD run, were conducted alternatively until a small hydrate nucleus in the cubic region had been generated. The induction time of hydrate nucleation required for the constrained MD method is typically longer than 0.5 μs. The nucleus is identified by calculating the number of hydrate cages formed in the constrained region, and the structure of the nucleus we obtained is amorphous (Figure 2).

Note that although the constraint would bias the nucleation dynamics, the constrained NVT process can generate a nucleus much faster, as it ignores the effect of environmental fluctuation. The word "faster" means the reduction of the computation time, but not the decrease of induction time of nucleation. Actually, confined system with a small volume might be difficult to nucleate than the bulk counterpart. By using this constrained method, however, we can avoid the expensive calculation of Coulomb interactions from plenty of environmental water molecules and, thus, significantly save the computational resources.

With the produced initial configurations containing a small seed of the gas hydrate (e.g., see Figure 2), an NpT relaxation
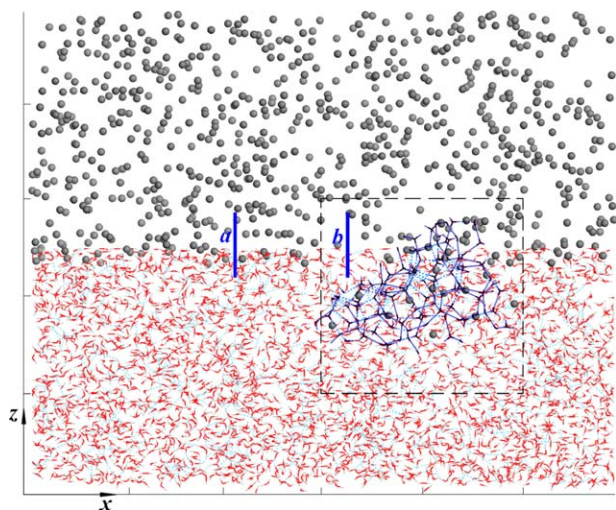
Figure 2. A typical initial configuration of our simulations on hydrate growth.

In the figure, H_2O molecules are shown by the stick model, and hydrogen bonds are represented by dashed lines. Guest molecules are represented by gray spheres, and the hydrate seed is denoted by the wire-frame model. The two blue bold lines, marked as *a* and *b*, denote two slices parallel to *yz*-plane used in Figure 6 to calculate density profiles. The black dashed-line frame denotes the unconstraint region during the constrained MD run performed to prepare the initial hydrate nucleus. [Color figure can be viewed in the online issue, which is available at wileyonlinelibrary.com]

process in unconstrained MD was performed at 275 K and 80–200 bar (for different guest molecules) for 4 ns, which was used to eliminate the effect of the artificial freezing process. Then, 500 ns unconstrained *NpT* MD runs were performed with a time step of 1 fs at the same thermodynamic conditions, to study the dependence of the detailed hydrate growth mechanism on the guest molecules. Although both the nuclei and the environment were free to thermally fluctuate in those simulation runs, the nuclei would grow gradually within the unconstrained MD runs because the initial nuclei produced by the constrained MD had already exceeded the size of critical nucleus. During the simulation runs, constant temperature and pressure were maintained by using the Nosé–Hoover algorithm.[36–38]

Results and Discussion

Adsorption of guest molecules on the nucleus surface

Previous studies[22,39] showed that the nucleation and growth of hydrate begins with adsorption of guest molecules on the faces of pentagonal or hexagonal rings formed with H_2O molecules. A similar tendency was observed in our simulations, as indicated by the probability of guest molecules (ε_2, σ_2) adsorbed on the face of hydrate rings (Figure 3). Because the hydrate nucleus was located at the vapor-liquid interface, we calculated separately the adsorption probabilities of guest molecules in the gas phase and liquid phase. From Figure 3, it is found that in the gas phase, guest molecules prefer to be adsorbed (mainly) on the face of pentagonal rings exposed to the gas phase, and roughly, each exposed hydrate ring adsorbs one guest molecule. However, in the liquid water phase, there are nearly no guest molecules adsorbed on the face of hydrate rings. The difference

is partly because of the limited solubility of guest molecules in the water phase due to the hydrophobic nature of the LJ guest molecules. Another possible reason for this difference is ascribed to the fact that, in comparison with the water phase, guest molecules diffuse more rapidly in the vapor phase and, thus, they can reach the face of the hydrate rings exposed to the gas phase more easily.

The adsorbed guest molecules play an important role in controlling crystal growth at the vapor-liquid interface. Hence, a question arises: do the adsorbed guest molecules behave the same as free ones? To answer this question, we first calculated the mean square displacement (MSD) curves of different guest molecules, and the results are given in Figure 4. The figure indicates that the mobility of guest molecules substantially decreases when adsorbed on hydrate rings, and the measured MSD is close to that of the enclosed guest molecules in hydrate cages.

It should be noted that similar results were observed for all the (ε, σ) parameters we investigated, although the figures presented are based on (ε_2, σ_2). Therefore, it is a common mechanism that the hydrate growth begins with adsorption of guest molecules on the face of hydrate rings, and the mobility of the adsorbed guest molecules is substantially reduced, similarly to the nucleation process suggested by Jacobson et al.[40] For the same reason, Jacobson et al.[40] recently suggested that the adsorbed guest molecules should be considered as a part of the crystal nucleus.

The effect of ε on crystal growth

In this section, we focus on the effects of ε on crystal growth by changing the parameter ε from 0.25 to 2.65 kJ/mol, with the molecular size $\sigma = 4.2$ Å. Because the intermolecular interaction between guest and water molecules becomes more
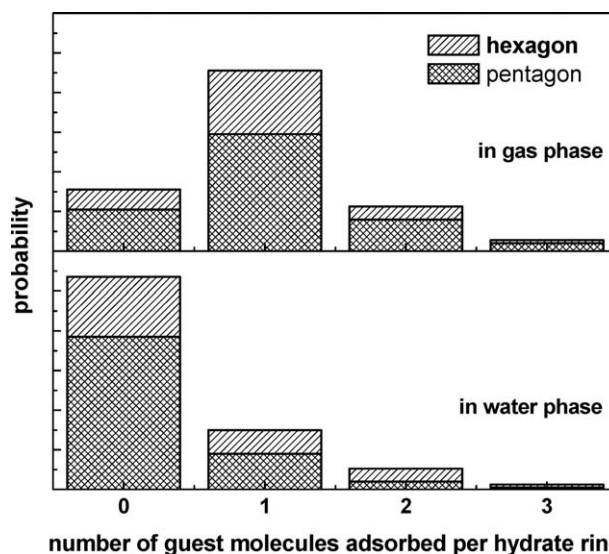

Figure 3. Probability of guest molecules (ε_2, σ_2) adsorbed on the face of hydrate rings at the external surface of the hydrate nucleus.

The probability was calculated from the number of guest molecules within a given distance of 4.5 Å to the center of the water rings at the external surface of the nucleus. Note that the hydrate rings on the nucleus surface can be identified by their relatively lower connecting index (number of hydrogen bonds), in comparison with those inside the nucleus.
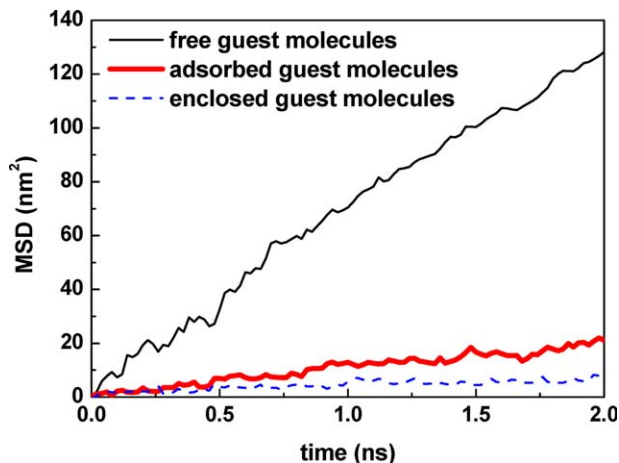
Figure 4. Mean square displacement (MSD) of guest molecules (ε_2, σ_2) in different status.

The MSD is calculated by averaging over 11 MSDs with different time origins, with an increment of 0.1 ns. [Color figure can be viewed in the online issue, which is available at wileyonlinelibrary.com]

Figure 5. Time evolution of the number of cages for the system with (a) low-soluble guest molecules and (b) high-soluble guest molecules.

The dashed line located at $z=0$ represents the initial phase interface at the beginning of the simulation, with $z>0$ being gas phase and $z<0$ being liquid water phase. [Color figure can be viewed in the online issue, which is available at wileyonlinelibrary.com]

attractive when ε increases, the solubility of guest molecules in water phase also increases with increasing ε.

The effects of the water–guest molecule interaction were first analyzed from the evolution of the number of hydrate cages and their distribution at the vapor-liquid interface (Figure 5). The results indicate that although the hydrate crystal grows along the vapor-liquid interface, a pronounced difference exists between the system with a weak water-guest molecule attraction (Figure 5a) and that with a strong attraction (Figure 5b). For the former system, the peak of cage distribution shifts toward the gas phase, but no obvious shift is observed for the system with the strong water-guest molecule attraction.

The difference between the two systems is ascribed to the difference of the solubility for guest molecules in the water phase. For the system with a weak water-guest molecule attraction (a small ε), as will be discussed below, the interface layer is relatively thin and the solubility of guest molecules in both the interface layer and the water phase is rather low (see Figure 6). In this work, the width of the interface layer is defined as a region where the densities of both the two components are more than half of their bulk density (see the inset of Figure 6b): the upper bound of the interface layer is located at the position that the density of water equals to half of the bulk water density, and similarly, the lower bound is at the position that the density of guest equals to half of the bulk guest density. The poorly mixing in interface layer and the low solubility of guest molecules inside the water phase prevent the nucleus from growing in the water phase. Instead, the nucleus appearing at the vapor-liquid interface gradually grows into vapor phase because of the availability of guest molecules. During the growth process, it is found that the free water molecules diffuse toward vapor phase along the surface of hydrate crystal (see the trajectories of H_2O molecules in Figure 7), and behave as a source of water molecules for the further hydrate growth. Then, the water molecules are located around the adsorbed guest molecules on the crystal surface, and form hydrogen bonds with other water molecules to complete the cage-enclosing process. Consequently, the hydrate grows along the phase interface and develops toward the gas phase. This
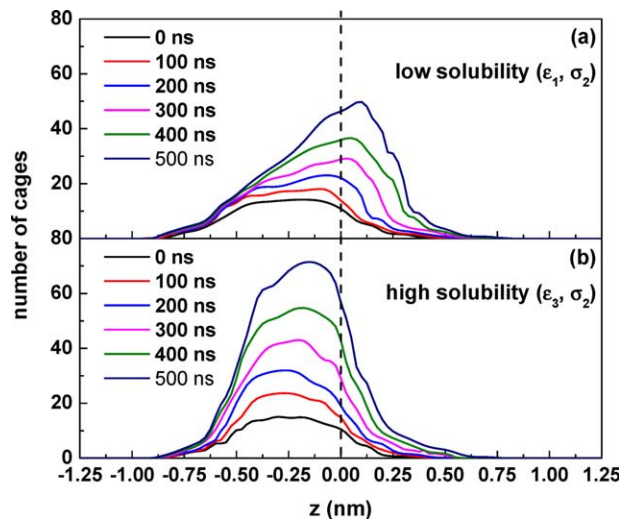
is the reason for the observation in Figure 5a that the peak of cage distribution shifts toward the gas phase for the system with a weak water-guest attraction.

However, for the system with a large ε, which corresponds to a strong water-guest molecule attraction, the trend is
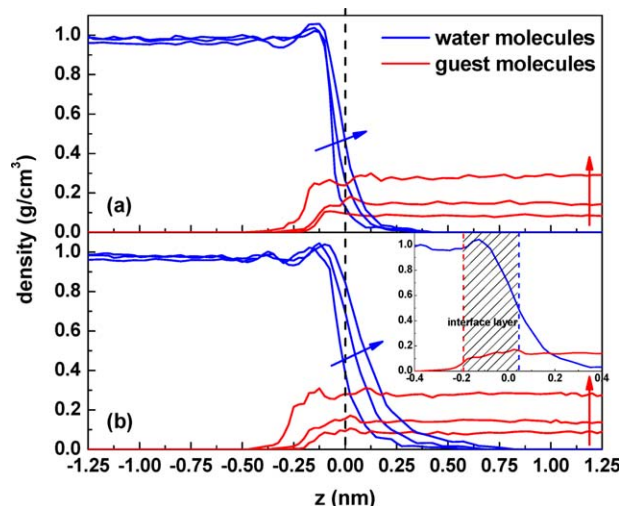

Figure 6. Density profiles of water and guest molecules along z-direction sampled (a) far from the crystal and (b) in the front of the crystal (see Figure 2).

Along the direction of the arrows, the value of ε (also the solubility of guest molecules) increases from ε_1 (0.65 kJ/mol), through ε_2 (1.45 kJ/mol), to ε_3 (2.25 kJ/mol), whereas the σ is fixed at σ_2 (4.2 Å). The dashed line located at $z=0$ represents the initial phase interface at the beginning of the simulation, with $z>0$ being gas phase and $z<0$ being liquid water phase. The inset of Figure 6b gives a schematic drawing of the interface layer. [Color figure can be viewed in the online issue, which is available at wileyonlinelibrary.com]
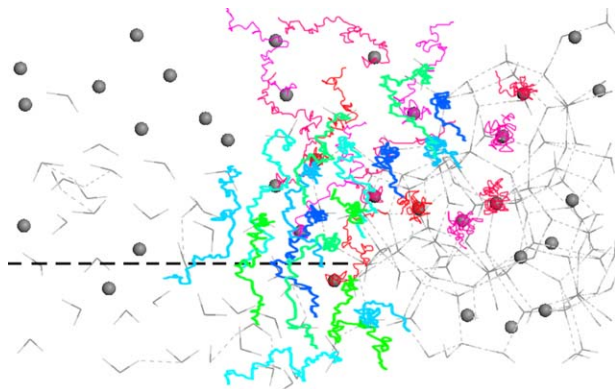
Figure 7. Trajectories of molecules near the surface of hydrate crystal for the system with guest molecules (ε_1, σ_2).

In the figure, the trajectories of H_2O molecules are denoted by thick curves, whereas those of guest molecules are shown by thin curves. The positions of the molecules shown in the figure correspond to the end of the trajectories. The dashed line represents the center of the initial phase interface. [Color figure can be viewed in the online issue, which is available at wileyonlinelibrary.com]

different: no obvious shift of cage distribution toward the vapor phase is observed. This is because the higher solubility of guest molecules at the interface layer and that in water phase provides a source of guest molecules for the hydrate growth. In this situation, different from the situation with a weak water-guest molecules attraction, the hydrate growth occurs mainly in the interface layer. For the same reason, the formation rate of hydrate crystal increases with the solubility of guest molecules (see Figures 5a, b). It should be noted that different water–guest molecule interactions would result in different values of the equilibrium formation temperature of the corresponding clathrate hydrates. Larger ε results in higher equilibrium formation temperature, or in other words, higher degree of supercooling at specified temperature. A high degree of supercooling is found to favor the formation of amorphous structure.[41] Therefore, although all our simulations were preformed at the same temperature of 275 K, for different systems the driving force for hydrate growth is actually different as a result of different degree of supercooling. The observation that hydrophilic guests will result in a faster growth of the hydrate crystal, can be understood as a result of high solubility and high supercooling, both of which are caused by the strong water–guest molecule interaction.

Our simulations also indicate that the structure of the interface layer, which affects the hydrate growth, is determined by the water–guest molecule interaction and influenced by the presence of the hydrate nucleus (Figure 6). With the increase of ε (along the direction of the arrows in Figure 6a), or equivalently the solubility of the guest molecules, the width of the interface layer would increase. Interestingly, we found that close to the hydrate crystal, the width of the interface layer increases further (Figure 6b).

The increase of the interface layer width near the hydrate could be interpreted as a result of the hydrophilic nature of the hydrate crystal. Because the hydrate crystal can be described as a hydrophilic cluster and it favors the water side at the phase interface,[32] it can move toward the water phase freely near the interface layer when it is small. How-

ever, a large cluster has less mobility to move itself. On the contrary, small water molecules can move themselves toward the large hydrate cluster to "wet" the cluster. As a result, the width of the interface layer increases further. The conjecture above can be also confirmed in Figure 6, which shows that widening of the interface layer is mainly due to the change of density profile of water molecules, rather than that of guest molecules. Furthermore, the analysis of the center of the interface layer in Figure 6b also indicates that there exists a delicate difference: the center is located at guest side ($z>0$) for a small ε, but at $z=0$ roughly for a large ε.
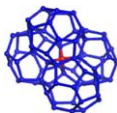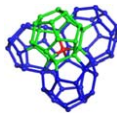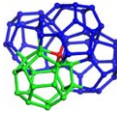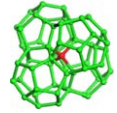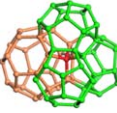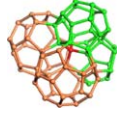
Finally, we must point out that our observation on the dynamic pathway of hydrate growth is in molecular (nanometer) scale: for the system with a weak water-guest molecule attraction, the diffusion of free water molecules from the liquid phase to the gas p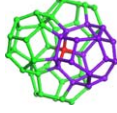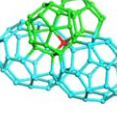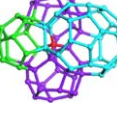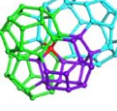hase along the hydrate surface is required for the hydrate growth. Nevertheless, in micrometer scale of experimental observations, water molecules in the vapor phase required for hydrate formation would become gradually unavailable as the distance from the vapor-liquid interface increases, because the diffusion of the water molecules over a large distance becomes very slow. In other words, the shift of the hydrate toward the vapor phase could be observed only in the molecular scale, as the nucleus only grows from the locations where both the water and guest molecules are simultaneously available.

The effect of σ on crystal growth

The effects of molecular size on the crystal structure of hydrates were studied previously by von Stackelberg.[42] He found that with the increase of the size of guest molecules, the hydrate structure is changed from sII (both $5^{12}6^4$ and 5^{12} cages are filled), through sI and sII (only $5^{12}6^4$ cages are filled), to sH. As to the issue of how the size of the guest and its solubility affect the nucleation pathways and initial structure of hydrate nuclei, Jacobson et al.[24] found that the overall nucleation mechanism for all guests is similar, and there are multiple competing channels to form the nuclei. The structure of the nuclei, on the other hand, is mainly determined by the size of guest molecules, rather than the cage composition or ordering of the stable or metastable hydrate crystals. In contrast to hydrate nucleation, how the size of guest affects the growth of the hydrate crystal is still not fully understood, because of the limitation of experimental monitoring techniques[43–45] and the difficulty of simulation methods to distinguish different structures in an amorphous crystal.[20,22,23,40,46–48]

Here, we investigated the effects of the size of guest molecules by changing the parameter σ from 2.1 to 6.3 Å, while the depth of potential well was fixed to $\varepsilon=1.45$ kJ/mol. To determine whether a hydrate cage belongs to sI, sII, or sH domains, we modified the vertex perception algorithm originally developed by Jacobson et al.[41,49] to identify sH domains. Each water molecule in the hydrate crystals is denoted by an array of (i, j, k, l, m), where the indexes i, j, k, l and m are respectively the number of 5^{12}, $5^{12}6^2$, $5^{12}6^4$, $5^{12}6^8$, and $4^35^66^3$ cages containing this water molecule. Because the water molecules in the hydrate are tetracoordinated to four, other water molecules by hydrogen bonds, that is, a water vertex shared by four polyhedral cages, we can expect the summation of i, j, k, l, and m should be four. In hydrate crystals, vertices (04000) and (13000) belong to sI lattice,[49] and vertices (40000), (30100), and (20200) belong

Table 1. The Vertices in the sI, sII, and sH Crystals. [Color table can be viewed in the online issue, which is available at wileyonlinelibrary.com]

Vertex		Structure	Single Crystal Data			Symmetry
			Atomic Fractional Coordinates[1]			
sI	(04000)		0.0000	0.5000	0.2500	$D_{2d}(\bar{4}2m)$
	$(13000)_1$		0.1841	0.1841	0.1841	$C_3(3)$
	$(13000)_2$		0.0000	0.3100	0.1154	$C_s(m)$
sII	(40000)		0.1250	0.1250	0.1250	$T_d(\bar{4}3m)$
	(30100)		0.2187	0.2187	0.2187	$C_{3v}(3m)$
	(20200)		0.1823	0.1823	0.3693	$C_s(m)$
sH	(30001)		0.6667	0.3333	0.3643	$C_{3v}(3m)$
	(20020)		0.8680	0.1320	0.5000	$C_{2v}(mm)$
	(10012)		0.6139	0.6139	0.1373	$C_s(m)$
	(20011)		0.7910	0.2090	0.2776	$C_s(m)$

In each structure, the center vertex of water molecule is shown in red, and the 5^{12}, $5^{12}6^2$, $5^{12}6^4$, $5^{12}6^8$ and $4^35^66^3$ cages are colored as green, blue, orange, cyan, and purple, respectively.
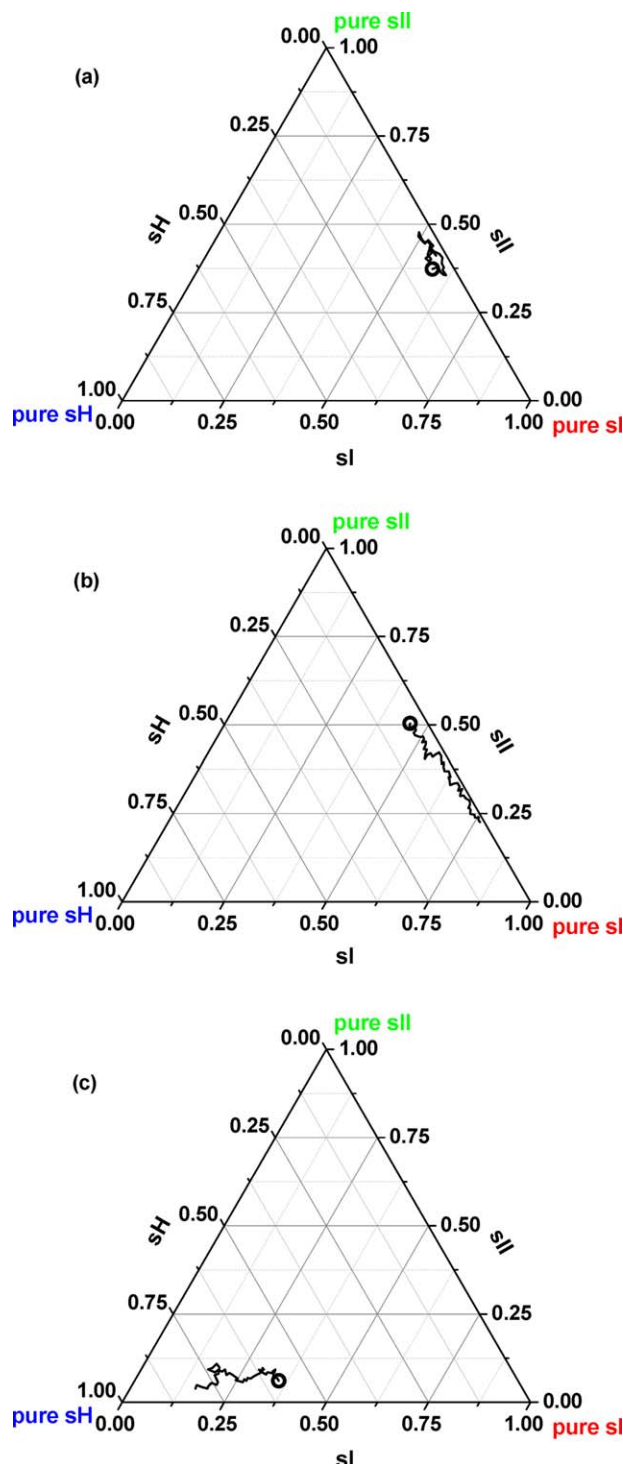
Figure 8. **Time evolution of cage components of the amorphous crystal for the system with (a) small size guest molecules σ_1, (b) middle size guest molecules σ_2, and (c) large size guest molecules σ_3.**

The initial positions of cage components are marked with circles. [Color figure can be viewed in the online issue, which is available at wileyonlinelibrary.com]

to sII lattice.[49] For sH lattice, there exist four kinds of vertices, that is, (30001), (20020), (10012), and (20011). Table 1 summarizes the vertices in the sI, sII, and sH crystals, respectively. After the assignment of water molecules in

hydrate, we can obtain the number of water molecules belong to sI, sII, and sH domains, that is, $n(\mathrm{sI})$, $n(\mathrm{sII})$, and $n(\mathrm{sH})$, respectively. However, it should be noted that not all water vertices in a hydrate nucleus can be decomposed into these three structures: there may exist some pieces in the nuclei remaining unclassified owing to its amorphousness.

Figure 8 shows the composition evolutions of different amorphous hydrate nuclei during their growth process. The location of hydrate composition is represented in this work by the fractional coordination of $(n(\mathrm{sI})/n, n(\mathrm{sII})/n, n(\mathrm{sH})/n)$, with $n = n(\mathrm{sI}) + n(\mathrm{sII}) + n(\mathrm{sH})$. For the small guest molecules (Figure 8a), the initial nuclei are of amorphous structure with the mixing sI and sII cages (nearly having no sH cages). The composition evolution (Figure 8a) shows that no favorable structure could be recognized at the end of the simulation run of 500 ns. This observation means that the structure transform in this growth process is rather slow, or, the mixing structure is thermodynamically stable. For the guest molecules of the middle size, however, the nucleus grows from the initial amorphous structure and gradually transforms into a structure dominated by sI unit cells (Figure 8b). The trend of structure evolution is consistent with the thermodynamic-phase diagram of Matsumoto and Tanaka,[50] in which the sI structure is the thermodynamic stable at this guest size. This observation suggests that the growth of the sI polymorph is always favored over that of the sII crystal, and the nucleus may finally grow into an amorphous hydrate dominated by sI unit cells. For the large guest molecules, the nucleus grows into a structure dominated by sH structure instead (Figure 8c).

In general, it is found from our simulations that except for some cases, such as $(\varepsilon_2, \sigma_1)$ in Figure 8a, the nucleus tends to evolve into a certain favorite hydrate structure as the hydrate nucleus grows. To describe the dependence of the preferable structure on the LJ parameters (ε, σ), we show a
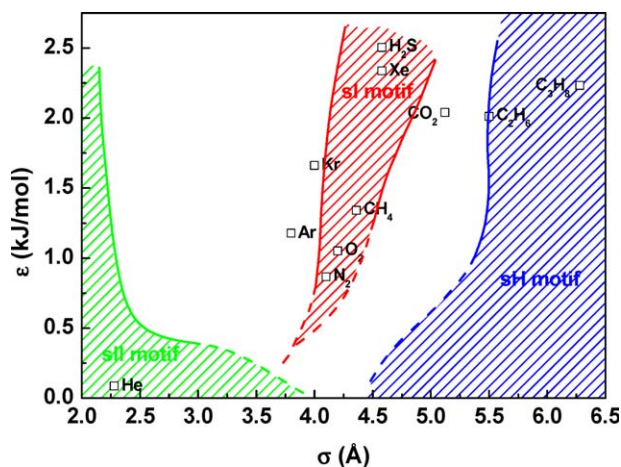

Figure 9. **Dynamic-phase diagram of the amorphous crystal.**

The dashed part of the curves corresponds to the situations that the cage component cannot be exactly determined. Note that the phase diagram is build at constant temperature, therefore, different (ε, σ) would induce different degree of supercooling and hence different growth rates of gas hydrate. [Color figure can be viewed in the online issue, which is available at wileyonlinelibrary.com]

dynamic-phase diagram in Figure 9. The phase diagram gives the dynamically preferable structures of hydrate growth processes, which is determined by the component with a fraction more than 50% at the end of 500 ns simulations.

From Figure 9, we can find that the dynamically preferable structure is determined, in general, by the value of σ, rather than the water-guest molecule attraction ε. The figure shows that a small σ usually leads to the sII-motif nucleus, and the hydrate structure changes into sI-motif with the increase of σ However, if σ is large enough the nucleus would turn into sH-motif. From the dynamic-phase diagram, we can predict the tendency for the composition evolution of amorphous hydrate nuclei (as shown in Figure 8) and its dependence on the properties of the guest molecule, namely the parameter (ε, σ). Interestingly, the figure shows that the dynamically preferable structure is basically consistent with the thermodynamically stable structure.[50] Another observation is that there exist regions in which the dynamically preferable structures cannot be determined, at least at the time scale we simulated. As a result, the observation in Figure 8a that no favored structure was found can be interpreted now: the parameters (ε, σ) happen to be located in the range between sI-motif and sII-motif (Figure 9).

Conclusions

In this work, systematic MD simulations were performed to illustrate the role of guest molecules played in the process of hydrate growth at vapor-liquid interface. Here, guest molecules were represented by a commonly used single-site LJ model, and our simulations spanned a large range of LJ parameters (ε, σ). In general, our simulations first reveal that the hydrate growth begins with the adsorption of guest molecules on the face of hydrate rings with reduced mobility. Then, the roles of guest molecules in the hydrate growth are investigated from the effect of the water–guest molecule attractive interaction ε and that of molecular size σ, respectively.

Our simulation results demonstrate that the water-guest molecule attraction regulates the pathway and rate of nucleus growth. For the system with a weak water-guest attraction ε, the poor molecule mixing in the interface layer and the low solubility of guest molecules inside the water phase prevent the nucleus from growing in the water phase. Instead, the free water molecules diffuse toward vapor phase along the surface of the hydrate crystal, and consequently, the hydrate grows along the phase interface but develops toward the gas phase. However, for the system with a large ε, which corresponds to a strong water-guest attraction, the trend is different: no obvious shift of hydrate clusters toward the vapor phase is observed. This is because there are sufficient guest molecules for the hydrate growth both in the water phase and at the interface layer. Another observation for the effect of the water-guest molecule attraction is that at constant temperature a strong water-guest molecule attraction, corresponding to a high degree of supercooling, often results in a higher rate of the hydrate growth and a less ordered structure.

As to the effects of the size of guest molecules, we find that at constant temperature the dynamically preferable structure is, in general, determined by the molecular size σ, rather than the water-guest molecule attraction. A small value of σ usually leads to sII-motif structures, and with the increase of σ the hydrate structure would gradually change into sI-motif. When σ is large enough the hydrate nucleus would develop into sH-motif. The obtained dynamic-phase diagram in the

(ε, σ) plane demonstrates that the dynamically preferable structure from our simulations is basically consistent with the thermodynamically stable hydrate structure.

It should be noted that we investigated here the hydrate growth process with different guest molecules, covering a wide range of LJ parameters (ε, σ). However, not all the guest molecules could be well-described by a single-site LJ potential. For example, the potential ignores the partial charge and the geometric anisotropy of guest molecules, which may become important factors in some situations.

Literature Cited

1. Sloan ED, Koh CA. Clathrate Hydrates of Natural Gases, 3rd ed. Boca Raton, FL: CRC Press, 2008.
2. Buffett BA. Clathrate hydrates. *Annu Rev Earth Planet Sci.* 2000;28:477–507.
3. Vatamanu J, Kusalik PG. Unusual crystalline and polycrystalline structures in methane hydrates. *J Am Chem Soc.* 2006;128:15588–15589.
4. Yang L, Tulk CA, Klug DD, Moudrakovski IL, Ratcliffe CI, Ripmeester JA, Chakoumakos BC, Ehm L, Martin CD, Parise JB. Synthesis and characterization of a new structure of gas hydrate. *Proc Natl Acad Sci USA.* 2009;106:6060–6064.
5. Lee H, Lee JW, Kim DY, Park J, Seo YT, Zeng H, Moudrakovski IL, Ratcliffe CI, Ripmeester JA. Tuning clathrate hydrates for hydrogen storage. *Nature.* 2005;434:743–746.
6. McElwain JC, Wade-Murphy J, Hesselbo SP. Changes in carbon dioxide during an oceanic anoxic event linked to intrusion into Gondwana coals. *Nature.* 2005;435:479–482.
7. Florusse LJ, Peters CJ, Schoonman J, Hester KC, Koh CA, Dec SF, Marsh KN, Sloan ED. Stable low-pressure hydrogen clusters stored in a binary clathrate hydrate. *Science.* 2004;306:469–471.
8. Sloan ED. Fundamental principles and applications of natural gas hydrates. *Nature.* 2003;426:353–363.
9. Bohannon J. Weighing the climate risks of an untapped fossil fuel. *Science.* 2008;319:1753.
10. Park Y, Kim DY, Lee JW, Huh DG, Park KP, Lee J, Lee H. Sequestering carbon dioxide into complex structures of naturally occurring gas hydrates. *Proc Natl Acad Sci USA.* 2006;103:12690–12694.
11. Kvenvolden KA. Potential effects of gas hydrate on human welfare. *Proc Natl Acad Sci USA.* 1999;96:3420–3426.
12. Dyadin YA, Larionov EG, Manakov AY, Zhurko FV, Aladko EY, Mikina TV, Komarov VY. Clathrate hydrates of hydrogen and neon. *Mendeleev Commun.* 1999;9:209–210.
13. Mao WL, Mao HK, Goncharov AF, Struzhkin VV, Guo Q, Hu J, Shu J, Hemley RJ, Somayazulu M, Zhao Y. Hydrogen clusters in clathrate hydrate. *Science.* 2002;297:2247–2249.
14. Mao WL, Mao HK. Hydrogen storage in molecular compounds. *Proc Natl Acad Sci USA.* 2004;101:708–710.
15. Liang S, Kusalik PG. Crystal growth simulations of H_2S hydrate. *J Phys Chem B.* 2010;114:9563–9571.
16. Liang S, Kusalik PG. Exploring nucleation of H_2S hydrates. *Chem Sci.* 2011;2:1286–1292.
17. Booker RD, Koh CA, Sloan ED, Sum AK, Shalaev E, Singh SK. Xenon hydrate dissociation measurements with model protein systems. *J Phys Chem B.* 2011;115:10270–10276.
18. Jiang H, Jordan KD. Comparison of the properties of xenon, methane, and carbon dioxide hydrates from equilibrium and nonequilibrium molecular dynamics simulations. *J Phys Chem C.* 2010;114:5555–5564.
19. Moon C, Taylor PC, Rodger PM. Molecular dynamics study of gas hydrate formation. *J Am Chem Soc.* 2003;125:4706–4707.
20. Hawtin RW, Quigley D, Rodger PM. Gas hydrate nucleation and cage formation at a water/methane interface. *Phys Chem Chem Phys.* 2008;10:4853–4864.
21. Zhang JF, Hawtin RW, Yang Y, Nakagava E, Rivero M, Choi SK, Rodger PM. Molecular dynamics study of methane hydrate

formation at a water/methane interface. *J Phys Chem B*. 2008;112:10608–10618.

22. Walsh MR, Koh CA, Sloan ED, Sum AK, Wu DT. Microsecond simulations of spontaneous methane hydrate nucleation and growth. *Science*. 2009;326:1095–1098.

23. Vatamanu J, Kusalik PG. Observation of two-step nucleation in methane hydrates. *Phys Chem Chem Phys*. 2010;12:15065–15072.

24. Jacobson LC, Hujo W, Molinero V. Nucleation pathways of clathrate hydrates: effect of guest size and solubility. *J Phys Chem B*. 2010;114:13796–13807.

25. Plimpton SJ. Fast parallel algorithms for short-range molecular dynamics. *J Comput Phys*. 1995;117:1–19.

26. Jorgensen WL, Chandrasekhar J, Madura JD, Impey RW, Klein ML. Comparison of simple potential functions for simulating liquid water. *J Chem Phys*. 1983;79:926–935.

27. Ryckaert JP, Ciccotti G, Berendsen HJC. Numerical integration of the cartesian equations of motion of a system with constraints: molecular dynamics of n-alkanes. *J Comput Phys*. 1977;23:327–341.

28. Hockney RW, Eastwood JW. Computer Simulation Using Particles. New York: Taylor & Francis, 1989.

29. Long JP, Sloan ED. Hydrates in the ocean and evidence for the location of hydrate formation. *Int J Thermophys*. 1996;17:1–13.

30. Smelik EA, King HE. Crystal-growth studies of natural gas clathrate hydrates using a pressurized optical cell. *Am Mineral*. 1997;82:88–98.

31. Subramanian S, Sloan ED. In: Proceedings of the Fourth International Conference on Gas Hydrates. Yokohama, Japan, 2002;856–861.

32. Mastny EA, Miller CA, de Pablo JJ. The effect of the water/methane interface on methane hydrate cages: the potential of mean force and cage lifetimes. *J Chem Phys*. 2008;129:034701(1–8).

33. Hawtin RW, Quigley D, Rodger PM. Gas hydrate nucleation and cage formation at a water/methane interface. *Phys Chem Chem Phys*. 2008;10:4853–4864.

34. Rodger PM. Stability of gas hydrates. *J Phys Chem*. 1990;94:6080–6089.

35. Kvamme B. Mechanisms for initiation of hydrate from liquid water liquid phase clustering, surface adsorbtion, or what? *Ann NY Acad Sci*. 1994;715:306–310.

36. Hoover WG. Canonical dynamics: equilibrium phase-space distributions. *Phys Rev A*. 1985;31:1695–1697.

37. Hoover WG. Constant-pressure equations of motion. *Phys Rev A*. 1986;34:2499–2500.

38. Melchionna S, Ciccotti G, Holian BL. Hoover NPT dynamics for systems varying in shape and size. *Mol Phys*. 1993;78:533–544.

39. Guo G, Zhang Y, Liu H. Effect of methane adsorption on the lifetime of a dodecahedral water cluster immersed in liquid water: a molecular dynamics study on the hydrate nucleation mechanisms. *J Phys Chem C*. 2007;111:2595–2606.

40. Jacobson LC, Hujo W, Molinero V. Amorphous precursors in the nucleation of clathrate hydrates. *J Am Chem Soc*. 2010;132:11806–11811.

41. Jacobson LC, Molinero V. Can amorphous nuclei grow crystalline clathrates? The size and crystallinity of critical clathrate nuclei. *J Am Chem Soc*. 2011;133:6458–6463.

42. von Stackelberg M. Feste gashydrate. *Naturwiss*. 1949;36:359–362.

43. Shen YR, Ostroverkhov V. Sum-frequency vibrational spectroscopy on water interfaces: polar orientation of water molecules at interfaces. *Chem Rev*. 2006;106:1140–1154.

44. Koh CA, Wisbey RP, Wu XP, Westacott RE, Soper AK. Water ordering around methane during hydrate formation. *J Chem Phys*. 2000;113:6390–6397.

45. Lehmkuhler F, Paulus M, Sternemann C, Lietz D, Venturini F, Gutt C, Tolan M. The carbon dioxide-water interface at conditions of gas hydrate formation. *J Am Chem Soc*. 2009;131:585–589.

46. Bai D, Zhang X, Chen G, Wang W. Replacement mechanism of methane hydrate with carbon dioxide from microsecond molecular dynamics simulations. *Energy Environ Sci*. 2012;5:7033–7041.

47. Bai D, Chen G, Zhang X, Wang W. Microsecond molecular dynamics simulations of the kinetic pathways of gas hydrate formation from solid surfaces. *Langmuir*. 2011;27:5961–5967.

48. Bai D, Chen G, Zhang X, Wang W. Nucleation of the CO_2 hydrate from three-phase contacty lines. *Langmuir*. 2012;28:7730–7736.

49. Jacobson LC, Matsumoto M, Molinero V. Order parameters for the multistep crystallization of clathrate hydrates. *J Chem Phys*. 2011;135:074501(1–7).

50. Matsumoto M, Tanaka H. On the structure selectivity of clathrate hydrates. *J Phys Chem B*. 2011;115:8257–8265.